QUARTERLY JOURNAL OF THE ROYAL METEOROLOGICAL SOCIETY
Q. J. R. Meteorol. Soc. **133**: 579–594 (2007)
Published online in Wiley InterScience
(www.interscience.wiley.com) DOI: 10.1002/qj.52

Investigation of a sea breeze front in an urban environment†

William T. Thompson,* Teddy Holt and Julie Pullen
Naval Research Laboratory, Marine Meteorology Division, Monterey, CA, USA

ABSTRACT: The dynamics of a sea breeze front interacting with the heavily urbanized New York City area are examined. In addition, we investigate the impact of the urban-influenced sea breeze front on transport and diffusion of simulated passive tracer plumes. We employ the U. S. Navy's Coupled Ocean/Atmosphere Mesoscale Prediction System (COAMPS® – a registered trademark of the Naval Research Laboratory) to perform a nested simulation with data assimilation for the sea breeze event of 9 August 2004. Available surface and upper-air observations are used to validate the simulation. We also perform a sensitivity study in which the urban influence is removed (no-urban).

The sea breeze front has characteristics of a density current, including an elevated head at the leading edge. The density current moves slowly and unevenly across the city. Kelvin–Helmholtz billows form in the region of the density current head, and the results show evidence of the occurrence of Kelvin–Helmholtz instability (KHI). The density current head is greatly elevated owing to the enhanced surface drag of the urban area. This urban influence is further explored in the no-urban simulation, in which the head of the density current is not elevated to the same degree and KHI does not occur.

The sea breeze/density current has a large impact on transport and diffusion of simulated tracer plumes, not only changing the direction of plume motion due to the wind shift but also redistributing tracer material in the vertical so as to produce dramatic, rapid changes in near-surface concentration as the front passes. In particular, large upward vertical velocity at the head of the density current advects tracer material to large elevations, greatly reducing near-surface concentration. After passage of the front, tracer is released into the shallow density current and confined near the surface, enhancing near-surface concentrations. KHI results in turbulent mixing at the upper surface of the plume, allowing for a small reduction in near-surface concentration. Published in 2007 by John Wiley & Sons, Ltd.

KEY WORDS sea breeze front; urban canopy; Kelvin–Helmholtz instability

Received 13 June 2006; Revised 12 October 2006; Accepted 7 February 2007

1. Introduction

Sea breezes, which are nearly ubiquitous in coastal locations throughout the world, feature prominently in the literature. Writing on sea breezes dates back to the time of Ancient Greece. Sea breezes have been discussed by Aristotle (330 BC), Francis Bacon (1664), and Immanuel Kant (1755), among others (a review is given by Miller *et al*., 2003). Given that sea breezes have a dramatic impact on local climate and air quality and that nearly one-half of the world's population lives in coastal areas, it is little wonder that sea breezes continue to garner significant attention.

In the present study, we investigate the nature of the sea breeze and associated circulations in the urban coastal environment of metropolitan New York City (NYC) using a high resolution mesoscale model with a parameterized urban canopy. Hereafter, we will refer to the sea breeze and associated circulations as the sea breeze complex (SBC), following Miller *et al*. (2003). A second objective of the present study is to examine the impact of the SBC on dispersion of passive tracers released in the urban coastal environment. We will also investigate sensitivity of the SBC to the presence of the urban canopy.

Sea breezes are one of a fairly large class of geophysical flows (including thunderstorm outflow, lake breezes, turbidity currents, avalanches, and pyroclastic flows) that can be characterized as density currents or gravity currents (Simpson *et al*., 1977; Sha *et al*., 1991; Reible *et al*., 1993; Wood *et al*., 1999; Lapworth, 2000; Miller *et al*., 2003), in which the cool, dense fluid from over the ocean displaces warmer air over land. The leading edge of the cool air has a raised head because of the updraught due to convergence. The height of the head is approximately twice that of the feeder flow (Simpson *et al*., 1977; Sha *et al*., 1991; Miller *et al*., 2003). The speed with which the density current advances into the ambient fluid is given by Miller *et al*., (2003) as:

$$|U| = k\sqrt{\frac{\Delta\rho}{\rho} g d}, \tag{1}$$

where U is the speed with which the dense fluid advances into the ambient flow, k is a constant, ρ is the density of the more dense fluid, $\Delta\rho$ is the density contrast across the front, g is the acceleration due to gravity, and d is the depth of the density current head. Thus, the

* Correspondence to: Dr William T. Thompson, Naval Research Laboratory, Marine Meteorology Division, Monterey, CA, USA.
E-mail: thompson@nrlmry.navy.mil

speed at which the density current advances is directly proportional to the square root of the density contrast and the depth and inversely proportional to the square root of the density of the more dense fluid.

The horizontal thermal contrast between cool marine air and warm continental air is often sharp and takes on a frontal character (Simpson *et al*., 1977; Sha *et al*., 1991; Zhong and Takle, 1992; Rao *et al*., 1999; Miller *et al*., 2003), although turbulent mixing of the dense fluid with the ambient fluid often impedes frontogenesis. Reible *et al*. (1993) derive the following dimensionless quantity, which characterizes the tendency toward sea breeze frontogenesis:

$$N_f = \frac{H}{w^*}\frac{\partial u}{\partial x} \sim \frac{H}{w^*}\frac{(U_2 - U_1)}{L_f}, \qquad (2)$$

where H is the mixed layer depth, w^* is the convective velocity scale, $(U_2 - U_1)$ is the difference in wind speed across the front, and L_f is the length over which the curvature of the density gradient occurs. N_f is formulated such that rapid frontogenesis is expected for large values of N_f (in the study of Reible *et al*. the most rapid frontogenesis was associated with $N_f = 1.25$). N_f can also be written as the ratio of the time-scale for frontal formation to the time-scale required for turbulent mixing to mix the dense fluid over the depth of the mixed layer. The frontogenesis function of Miller (1948) can be used to determine the relative contributions of frontogenetic forcing terms (Kraus *et al*., 1990; Arritt, 1993). Miller *et al*. (2003) derive a frontogenetic function specific to the sea breeze front.

In a sea breeze front, strong wind shear and the large vertical thermal gradient between the dense fluid and the overlying ambient air can result in KHI and the associated KH billows (Sha *et al*., 1991; Nielson, 1992; Reible *et al*., 1993; Rao *et al*., 1999; Miller *et al*., 2003). KH billows form when the Richardson number (Ri) <0.25. Under certain flow conditions KH billows will become unstable, forming vortices, which propagate upwind over the dense fluid. These vortices promote mixing of the dense fluid with the ambient air.

In a two-dimensional sea breeze modelling study by Sha *et al*. (1991), a series of vortices form along the zero-velocity boundary (the boundary between on-shore and off-shore flow) and propagate backwards relative to the front, over the trailing flow. Note that the thermal internal boundary layer does not coincide precisely with the zero-velocity boundary, although they are close. A region of $0 < \mathrm{Ri} \leq 0.25$ lies along the thermal internal boundary layer, providing evidence that the vortices are the result of KHI. The amplitude of the KH billows is 700 m and the wavelength is 0.5–3.0 km with a typical value of 1.5 km.

KHI does not occur at all stages of sea breeze frontal evolution. When it does occur, KH billows are generated in the front of the head, 'roll-over' and form vortices, and the vortices are transported backward along the zero-velocity boundary. The vortices enhance mixing between the dense fluid and ambient fluid, slowing the advance of the front and thereby acting as 'top friction'. Sha *et al*. (1991) analyse time series of the terms of the momentum budget for a control volume within the frontal zone. The relevant forces are the pressure gradient force, surface friction, top friction induced by KHI, and the residual. The pressure gradient is dominant at all times, but the frictional forces change in relative magnitude – the top friction is larger than the surface friction from mid-afternoon to early evening and the bottom friction is larger in the early morning and late evening. These top friction effects explain the often observed slowing of the front during the afternoon.

Rao *et al*. (1999) performed a real-data, nested, three-dimensional simulation of sea and river breezes in central Florida with horizontal nest resolutions of 1.6 km, 400 m, and 100 m. The results from their second nest show vortices originating at the head of the Indian River Breeze and propagating backwards along the zero-velocity boundary at the upper surface of the dense fluid as in Sha *et al*. (1991). (The sea breeze does not enter the highest resolution nest in this study.) Although the major emphasis of the study is on horizontal roll vortices, the authors attribute the backward propagating vortices atop the dense fluid to KHI. They note that the Richardson number in the vicinity of the vortices ranges from 0.15 to 0.4 and that the wavelength of the KH billows in this study ranged from 600 m to 2.5 km.

In aircraft observations, Wood *et al*. (1999) find that turbulence behind the leading edge of a sea breeze front displays a wave-like structure with a wavelength of 1–3 km. The authors claim that these waves are not KHI, but rather solitary waves occurring as the density current interacts with a pre-frontal stable layer. The solitary waves propagate along the stable layer at a speed greater than that of the front. At the same time, gravity waves propagate rearward over the cold air. The authors speculate that the great inland travel distance and speed of SBCs in the evening and at night reported in the literature (Simpson *et al*., 1977; Physick, 1980; Miller *et al*., 2003) may actually be solitary waves rather than a SBC *per se*.

The interaction of sea breezes with heavily urbanized areas is discussed by several authors – both in terms of the enhanced surface drag and the interaction with the Urban Heat Island (UHI) (Gedzelman *et al*., 2003). For example, synoptic and sea breeze frontal passages can be frictionally retarded by 50% as they approach NYC (Loose and Bornstein, 1977; Bornstein and Thompson, 1981). Urban heating also appears to play a role in distorting near-surface temperatures as sea breeze fronts pass (Novak and Colle, 2006).

The SBC impacts air quality in several ways, including sea breeze fumigation, which occurs when elevated plumes are entrained into a growing convective internal boundary layer and are rapidly mixed to the surface (Lyons *et al*., 1981; Abbs and Physick, 1992; Zhong and Takle, 1992); stable or convective internal boundary layers, in which an internal boundary layer forms in onshore flow and greatly limits the mixing depth (Hsu,

1988; Stull, 1988); 'translocation', in which plumes encountering strong updraughts immediately ahead of the sea breeze front are vertically advected to large elevations (Lyons *et al*., 1995); and horizontal advection of pollution, either by recirculation in the sea breeze cell or by contamination of the density current itself (Bornstein and Thompson, 1981; Abbs and Physick, 1992).

There is a lack of detailed study of the interaction of KHI with complex urban environments and their impact on tracer distributions – both topics that are examined in the work described here. We present details on the non-hydrostatic mesoscale model used in the present study in section 2. In section 3, we discuss the results for sea breeze frontal evolution, the extent to which the results are consistent with KHI, and the impact of the sea breeze on the dispersion of a passive tracer quantity, and investigate the sensitivity of the results to the urban canopy parameterization. We present our conclusions in section 4.

2. Model description

2.1. General description

COAMPS® is a non-hydrostatic mesoscale modelling system, using multiple nests having different horizontal resolution. It features a full suite of physical parameterizations, including schemes for radiation, cloud microphysics, urbanization, and turbulence. Time-dependent lateral boundary conditions are obtained from the Navy Operational Global Atmospheric Prediction System (NOGAPS) and applied to the boundaries of the outermost nest. Lateral boundary conditions on inner child nests are supplied by the outer parent nest. Data assimilation is accomplished using a scheme which, in the absence of observational data, retains horizontal and vertical structure developed in the previous forecast in the initial conditions of a subsequent forecast. Where observational data are available, these data are incorporated into the initial conditions using an increment formed between the observational analysis and the previous forecast. The model is described in more detail by Hodur *et al*. (2002).

2.2. Model features

2.2.1. Physical parameterization schemes

In parameterizing boundary layer processes, COAMPS® uses a prognostic equation for turbulent kinetic energy (TKE) with diagnostic equations for other second moment quantities. The buoyant production of TKE is computed from the virtual buoyancy flux. The turbulent length scale is calculated using a Blackadar scheme. In stable conditions a length scale that uses a turbulence velocity scale and the Brunt–Vaisala period is used. The eddy coefficients are based on Yamada (1978), while surface fluxes and surface stress are computed from the Louis (1979) scheme. Cloud microphysics is parameterized following a modified Rutledge and Hobbs (1983) and Khairoutdinov and Kogan (2000) scheme. In this scheme, there are prognostic equations for six species of water substance: vapour, cloud water, rain, cloud ice, snow, and graupel. The COAMPS® microphysical species impact the radiative flux divergence. The long wave radiation incorporates the mixing ratio of cloud liquid water in the calculated emissivity. The short wave radiation scheme does not directly use mixing ratios of cloud water and ice but rather parameterizes the effect of clouds on optical depth (Harshvardhan *et al*., 1987).

2.2.2. Urban canopy parameterization

To represent the effects of the city on the mesoscale, an urban canopy parameterization (UCP) is used. The scheme used in COAMPS® is the multi-layer parameterization based on Brown and Williams (1998). The original implementation has been modified in COAMPS® by Chin *et al*. (2005) to include a roof top surface energy equation, and that implementation is used here.

This UCP is categorized as a multi-level parameterization because urban effects are computed vertically throughout the urban canopy. Thus, the urban canopy friction source is represented via modified aerodynamic drag in the momentum equations. Likewise, the thermal effects of the urban region are included through a modified thermodynamic equation that considers the heat fluxes from rooftop, street, and building wall reflections. Trapping of radiation in street canyons is considered as a non-prognostic anthropogenic heating term in the urban region. The urban canopy is treated as a source of turbulence production to account for turbulence wake generation of TKE via a modified TKE equation. The addition of a rooftop surface energy equation enables the parameterization to exhibit a more reasonable diurnal cycle of the heat island effect (Chin *et al*., 2005). Holt and Pullen (2007) give a more detailed description of the UCP.

Urban parameterizations require several input parameters to describe the morphology of the urban environment. For this study a combination of the United States Geological Survey (USGS) 24-category 1 km dataset and a gridded 250 m resolution database for Manhattan (Burian *et al*., 2005) is used. The determination of urban versus non-urban (or rural) regions, building heights, and plan area fractions is based on the 250 m database for Manhattan and the USGS database for suburban regions elsewhere. Over Manhattan, the tallest buildings are generally concentrated in midtown and lower Manhattan, with the maximum building height being approximately 200 m. For the suburban regions the building height uses the default 10 m value. Table I summarizes the urban canopy parameters.

2.3. Model configuration

In the present study, the model is run in a five-nest mode with horizontal resolutions of 36 km, 12 km, 4 km,

Published in 2007 by John Wiley & Sons, Ltd.

DOI: 10.1002/qj

Table I. Description of the urban canopy parameters for nests 4 and 5.

	Building height (m)	Urban fraction	Roof fraction	Anthropogenic heating (W m^{-2})	Urban drag (N m^{-2})
Manhattan and surrounding urban regions	Burian *et al*. (2005) See Figure 2	Burian *et al*. (2005)	Burian *et al*. (2005)	50	Building height * 0.0005
Suburban regions	10	0.2	0.1	20	0.01

1.333 km, and 0.444 km (Figure 1). The innermost nest consists of 106×166 grid points and spans a region of 47×73 km centred on Manhattan. In the vertical 60 levels are used from the surface to ~30 km with 13 grid points in the lowest 100 m and 29 levels below 1 km. The UCP is employed on nests 4 and 5. Figure 2 shows the urban regions and building heights for nest 5.

High-resolution hindcasts of water surface temperatures are obtained from the New York Harbor Observing and Prediction System (NYHOPS: Blumberg *et al*., 1999). NYHOPS is a three-dimensional coastal and estuary ocean model with level 2.5 Mellor Yamada turbulence closure based on the Princeton Ocean Model (Blumberg and Mellor, 1987). The model incorporates measured river discharge of 43 rivers and realistic specification of outflow from 110 water treatment facilities. Such discharges can enhance spatial inhomogeneities of water temperature. The resolution of NYHOPS is approximately 500 m in the New York Harbor region (including the Hudson and East River). NYHOPS has been extensively evaluated and shown to have significant skill in predicting ocean properties such as surface and subsurface temperature and salinity, currents, and water level (Fan *et al*., 2006). Time-varying (hourly) NYHOPS sea surface temperatures (SSTs) are used on nests 4 and 5.

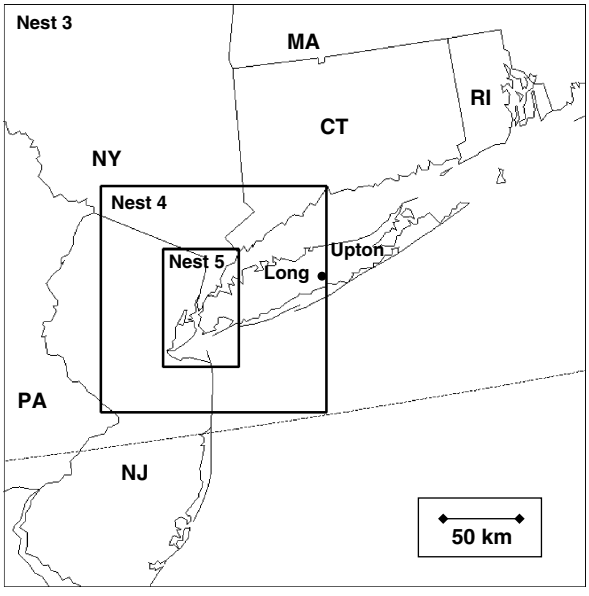

Figure 1. COAMPS model domain for inner nest 3 (4 km resolution), nest 4 (1.333 km), and nest 5 (0.444 km).

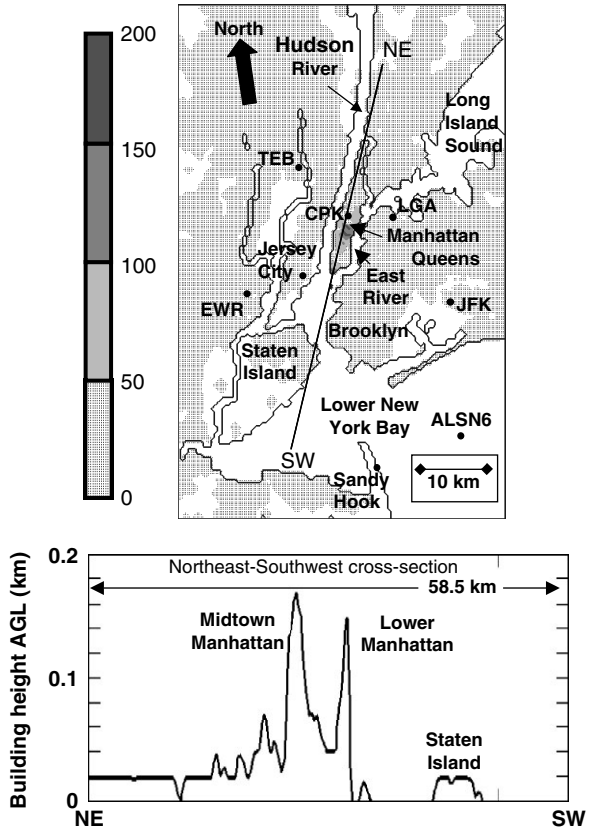

Figure 2. COAMPS nest 5 (0.444 km) building heights (shaded, metres) used in the urban parameterization (top) and along northeast–southwest (NE-SW) cross-section (bottom) with points of interest discussed in the text.

COAMPS® has been extensively validated over the NYC region using the same nesting strategy, urban canopy parameterization, and the NYHOPS SSTs (Pullen *et al*., 2007). The statistical evaluations performed show that the model faithfully reproduces many features of the mesoscale environment of the NYC area. The time-varying high resolution SSTs improve near-surface wind speed and air temperature prediction in the harbour region when compared with conventional sources of over-water bottom boundary specification. The NYHOPS SSTs, furthermore, produce local boundary layer modification (e.g. stable internal boundary layer formation) that is consistent with observations. The NYHOPS SST fields also contain the diurnal signature of SST evolution, which is expected to enhance this study. Since the NYHOPS SSTs have a demonstrated positive impact on model

performance, they are retained in the study presented here.

The period of focus for this study is 1200 UTC (0800 LT) 9 August to 1200 UTC (0800 LT) 10 August 2004 (LT = UTC − 4 h). Sea breeze evolution is closely tied to the diurnal cycle, thus, LT will be used hereafter. To properly spin up the boundary layer and mesoscale structure, a series of 12 h simulations are conducted for 5 days (3–9 August 2004) before the period of interest. The first simulation starting at 2000 LT 3 August 2004 uses initial fields interpolated from the one-degree NOGAPS to the COAMPS® domain. All subsequent forecasts use the previous COAMPS® 12 h forecast as initial conditions. At the beginning of each assimilation cycle (every 12 h), a three-dimensional multivariate optimum interpolation (MVOI) using quality-controlled data from radiosondes, surface stations, aircraft, and satellites is conducted to obtain an analysis blended from the observations and model first guess (12 h forecast; Hodur, 1997). During the data assimilation period and the period of interest, the UCP is active on grids 4 and 5. In addition, time-dependent water surface temperatures on these innermost nests are supplied by the NYHOPS hindcasts every hour.

3. Results

3.1. Synoptic setting

Figure 3 shows the synoptic setting for this investigation, in which a subset of the outermost nest (36 km resolution) shows the analyses of sea level pressure and 1000 hPa wind (Figure 3(a)) and the 500 hPa height and temperature (Figure 3(b)). The ridge at 500 hPa lies between troughs over the Canadian Maritimes and just to the west of the northern Great Lakes and the area is under light northwesterly (NW) flow. At the surface, a high is centred over the Carolinas and a 1000 hPa wind is westerly over the NYC area in association with the anticyclonic flow.

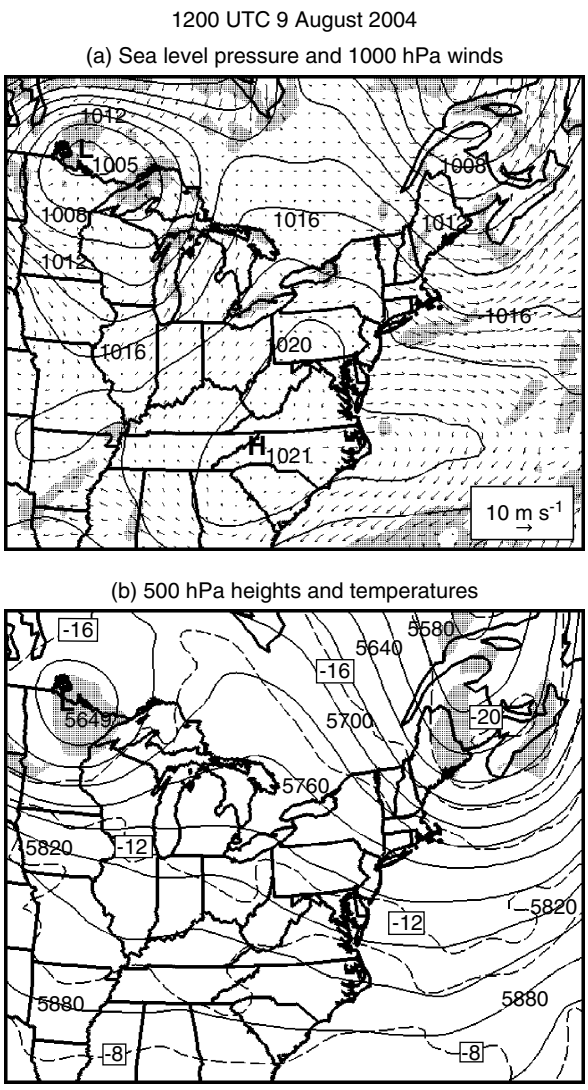

Figure 3. COAMPS nest 1 (36 km) analysis valid at 1200 UTC 9 August 2004 for a subset area focused on the eastern United States of (a) sea level pressure (solid line, interval = 2 hPa), 1000 hPa winds (arrows, shown every other grid point), and regions of horizontal convergence greater than 2.0×10^{-5} s^{-1} (shaded); and (b) 500 hPa geopotential heights (solid line, interval = 30 m), temperatures (dashed line, interval = 2 °C), and regions of absolute vorticity greater than 2.0×10^{-4} s^{-1} (shaded).

3.2. Sea breeze evolution

The first evidence of onshore flow begins at 1200 LT. Shown in Figure 4(a) are 10 m winds and 2 m potential temperature valid at 1200 LT. Several sea breeze boundaries are apparent within nest 5, including the one of primary interest moving ashore over Brooklyn and Queens, as well as those along the coast of Long Island Sound and near the harbour area. The existence of multiple sea breeze boundaries is consistent with the results of Novak and Colle (2006). Note that the sea breeze is locally forced, owing to a cold SST over western Lower New York Bay contrasted with increasing temperature over land. Strong divergence is apparent over the cold SST. This gives rise to south–southwesterly (SSW) onshore flow in Brooklyn. Southerly onshore flow due to the cold SST over Lower New York Bay has been noted in other studies of this area using the NYHOPS analyses (Pullen *et al.*, 2007), although, in simulations using the operational SST analysis, the SST is much warmer in this region, and southerly onshore flow is absent. At 1400 LT (Figure 4(b)), the SSW sea breeze has not penetrated significantly further inland. A much stronger large-scale sea breeze circulation, forced by large-scale land/ocean baroclinicity, is approaching from the south east. By 1500 LT (Figure 4(c)), the large-scale sea breeze moves onshore and the front begins to penetrate further inland. This evolution can be seen also in Figure 5, which shows isochrones of sea breeze frontal passage. At 1600 LT (Figure 4(d)), the primary front is over the central portion of Brooklyn and Queens moving toward the East River while another stronger front is moving over the Jersey City area of New Jersey owing to strong onshore flow from NY Harbor. There is also southerly flow over Manhattan Island due to flow from

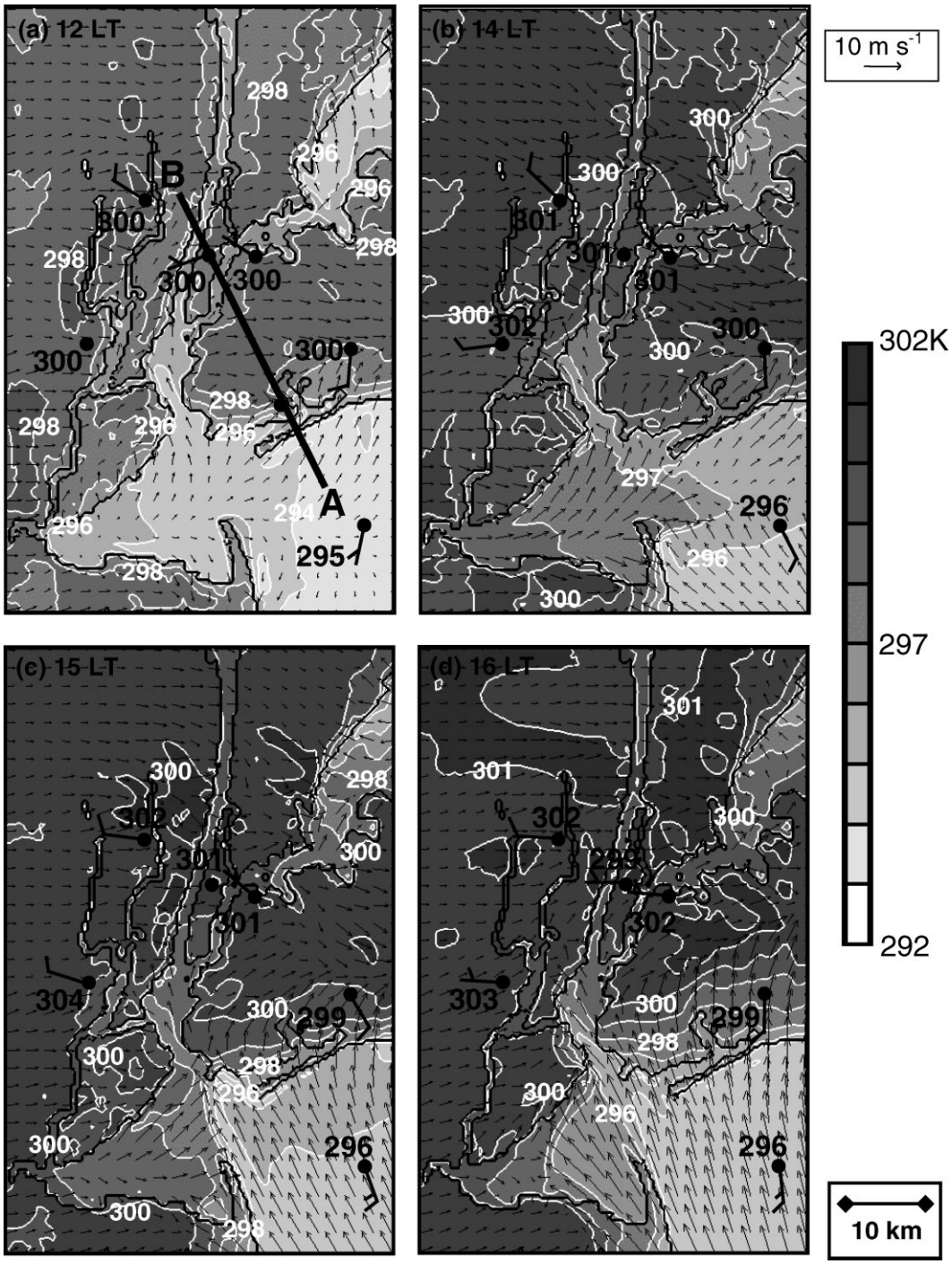

Figure 4. COAMPS nest 5 (0.444 km) simulation of 2 m potential temperatures (shaded, interval = 1 K) and 10 m winds (arrows, every fifth grid point) valid at (a) 12 LT; (b) 14 LT); (c) 15 LT; and (d) 16 LT 9 August 2004. Observations are plotted in black (temperature, K; winds full barb = 5 m s^{-1}). (LT is UTC − 4 h).

NY Harbor. At 1700 LT the primary front reaches the East River (Figure 5).

Observed wind direction and speed are indicated by wind barbs plotted in Figure 4(a)–(d). The observed 2 m temperature is also indicated in black, while model temperature contours are labelled in white. In Figure 4(a) (1200 LT), the SSW local-scale sea breeze is reflected in the observed wind at John F Kennedy (JFK) Airport (200° at 5 m s^{-1}), which is consistent with the model wind field. In Figure 4(b) (1400 LT), wind speeds have increased significantly and the pre-frontal wind has a strong westerly component. The observations also indicate a substantial northerly component which is under-represented by the model; i.e. the model winds are west–northwest (WNW) while the observations are north–northwest (NNW). The approaching large-scale sea breeze flow is shown by the Ambrose Light station (ALSN6) observation. At 1500 LT (Figure 4(c)), the observed wind at JFK turns SE, as does the model wind field at this location, consistent with the arrival of the

Published in 2007 by John Wiley & Sons, Ltd.

DOI: 10.1002/qj

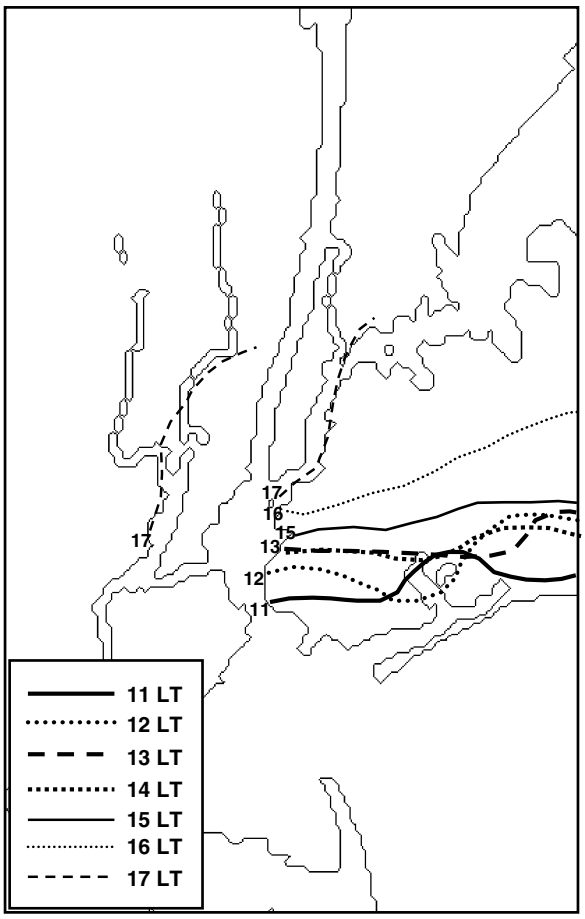

Figure 5. Isochrones of sea breeze frontal passage from 1100 to 1700 LT 9 August 2004 for COAMPS nest 5 (0.444 km) simulation.

large-scale sea breeze front. The observed wind at La Guardia (LGA) Airport is still westerly, indicating that the sea breeze front lies between these two locations. This is consistent with the model forecast. At 1600 LT (Figure 4(d)), the front has moved further inland but still has not reached LGA (the observed wind at LGA changes to SE at 1800 LT). Model temperatures tend to be ~1 K lower than observed at most locations but temperature evolution as the front progresses across the city is well represented by the model.

Figure 6 shows the observed and modelled time series of wind speed and direction and air temperature at JFK. The wind speed and direction are generally fairly well represented by the model, but the temperature is too low until 1400 LT. After 1400, the temperature error is less than one degree and the increase in wind speed is captured well by the model. The observations show SE flow at 1500, but the model at this location is still southwesterly (SW), though a large region of SE flow in the model is adjacent to the area (Figure 4(c)). After 1500 LT, the wind direction in both the model and the observations shifts to southerly as the wind speed increases to ~7 m s^{-1}.

Figure 7 shows the temporal evolution of the atmospheric vertical structure. The model skew-T log P thermodynamic diagram at the location of Upton, NY on

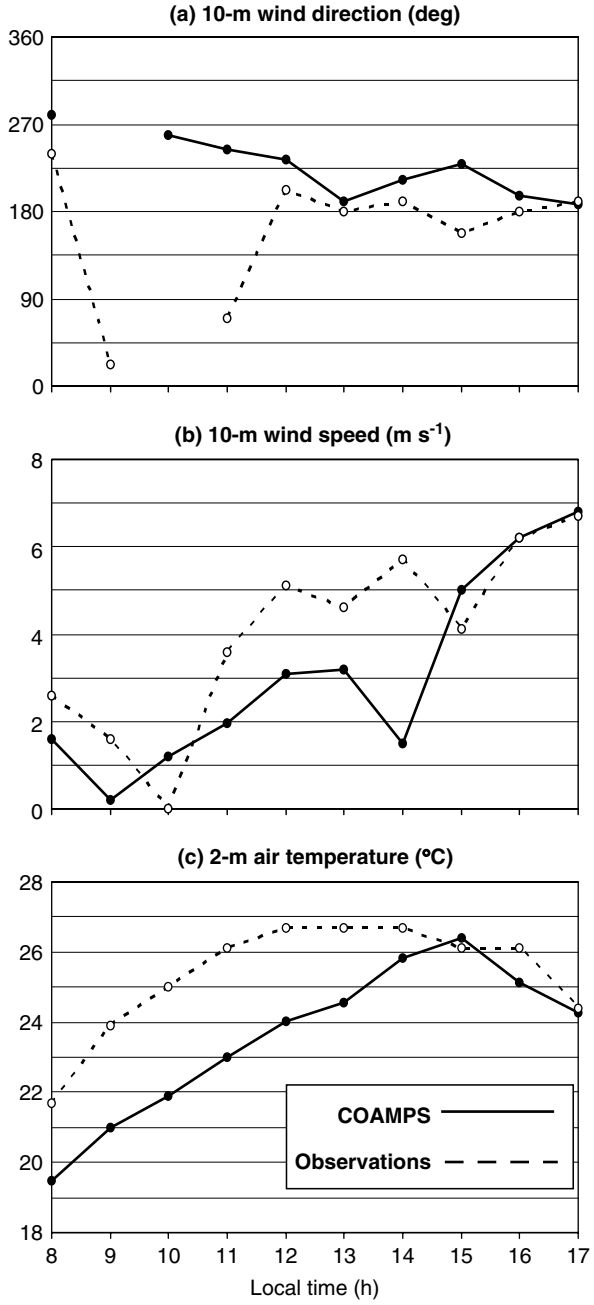

Figure 6. Time series from 0800 to 1700 LT 9 August 2004 at JFK airport for COAMPS (solid line) and observations (dashed line) of (a) 10 m wind direction (deg); (b) 10 m wind speed (m s^{-1}); and (c) 2 m air temperature (°C). Wind directions are not shown for the time periods of calm winds (<0.2 m s^{-1}).

Long Island from nest 3 (4 km resolution) is compared with the Upton sounding. Upton is 75 km to the east of the nest 5 eastern boundary but is the closest radiosonde location. Model simulations show close agreement in the temperature profile and agreement in the broad scale vertical structure of moisture. Note also that the depth of the boundary layer is well represented by the model.

The heavy black line in Figure 4(a) is the plane of the cross-section A–B that extends 41 km SE–NW from the Lower New York Bay, across Brooklyn and Manhattan into New Jersey. Figure 8(a) shows potential temperature

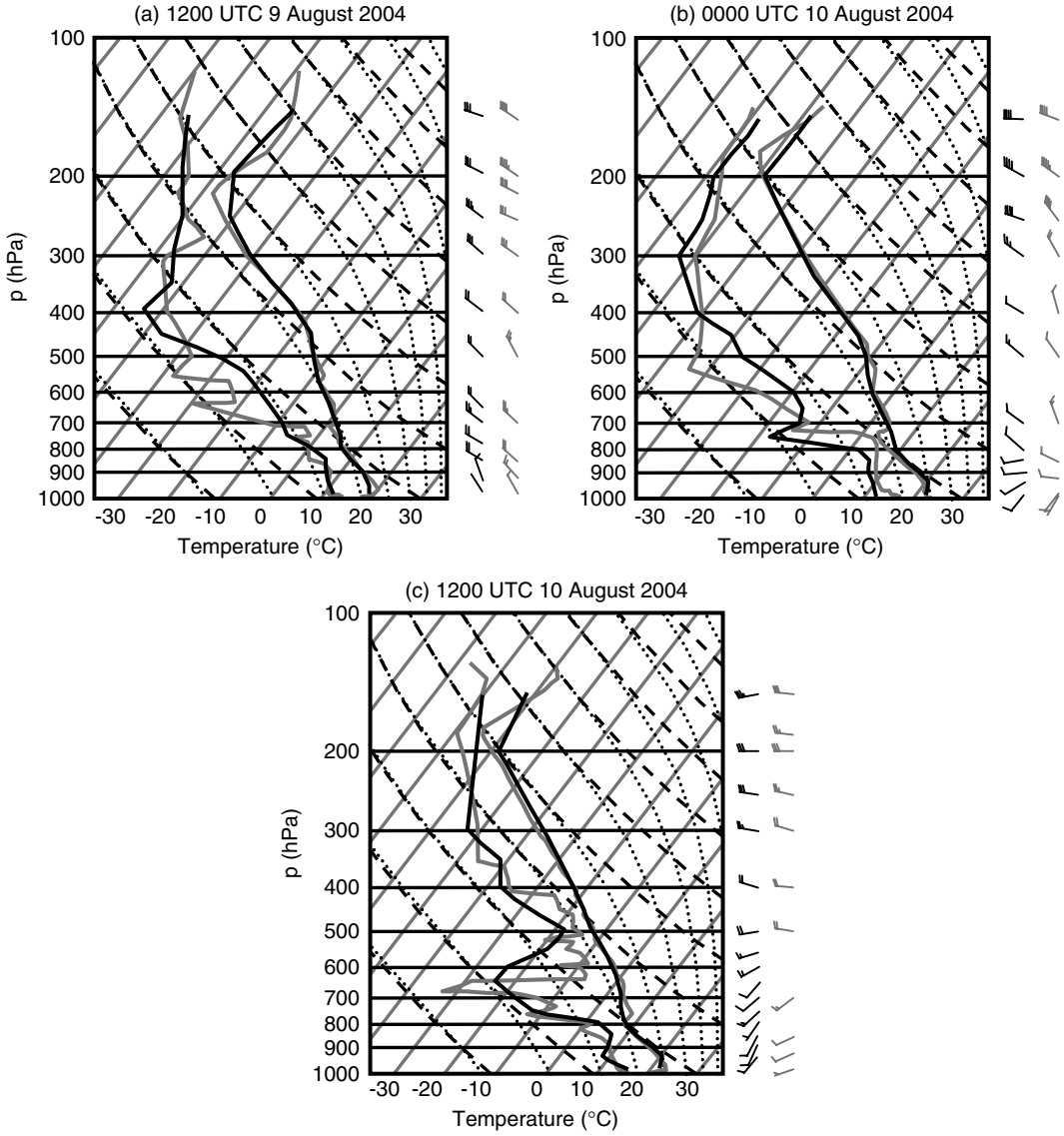

Figure 7. Skew-T log P plots at Upton, NY for observations (gray) and COAMPS nest 3 simulation (black) valid at (a) 1200 UTC 9 August (COAMPS analysis); (b) 0000 UTC 10 August (12 h forecast); and (c) 1200 UTC 10 August 2004 (24 h forecast).

and streamlines of flow in the plane of the cross-section extending from the surface to 1000 m at 1530 LT. Note the shallow density current entering the cross-section from the south east with the density current head at the leading edge and the vortex (V-1) above the dense fluid intrusion lagging the density current head. The depth of the head is highly variable with time but is frequently greater than twice that of the following flow, in contrast to previously published investigations in which the head is twice as deep as the following flow. This discrepancy may be attributable to the large surface drag over the urban area. At 1545 LT (Figure 8(b)), the head is roughly four times the depth of the dense fluid and two vortices are apparent; one near the density current head and one further to the rear. At 1600 LT (Figure 8(c)), the density current has progressed further inland and the head is still roughly four times the depth of the dense fluid. There is one large vortex (V-2) over the dense fluid. The vortices appear to be shed near the density current head and then to move rearward with respect to the density current. At 1615 LT (Figure 8(d)), the large vortex (V-2) seen at 1600 LT is just exiting the cross-section to the south while a new vortex (V-3) has just been shed near the density current head.

3.3. Kelvin–Helmholtz instability

As noted in the 'Introduction', KH billows are unstable to certain wind and mass configurations. To assess the stability of the flow, the Taylor–Goldstein equation for the vertical structure of vertical velocity can be used:

$$\frac{\partial^2 w}{\partial z^2} + \Lambda(z) w = 0. \tag{3}$$

The derivation of a criterion for instability in this case is given in Appendix A:

$$\frac{\partial^2 U \Big/ \partial z^2}{Nk} < 2. \tag{4}$$

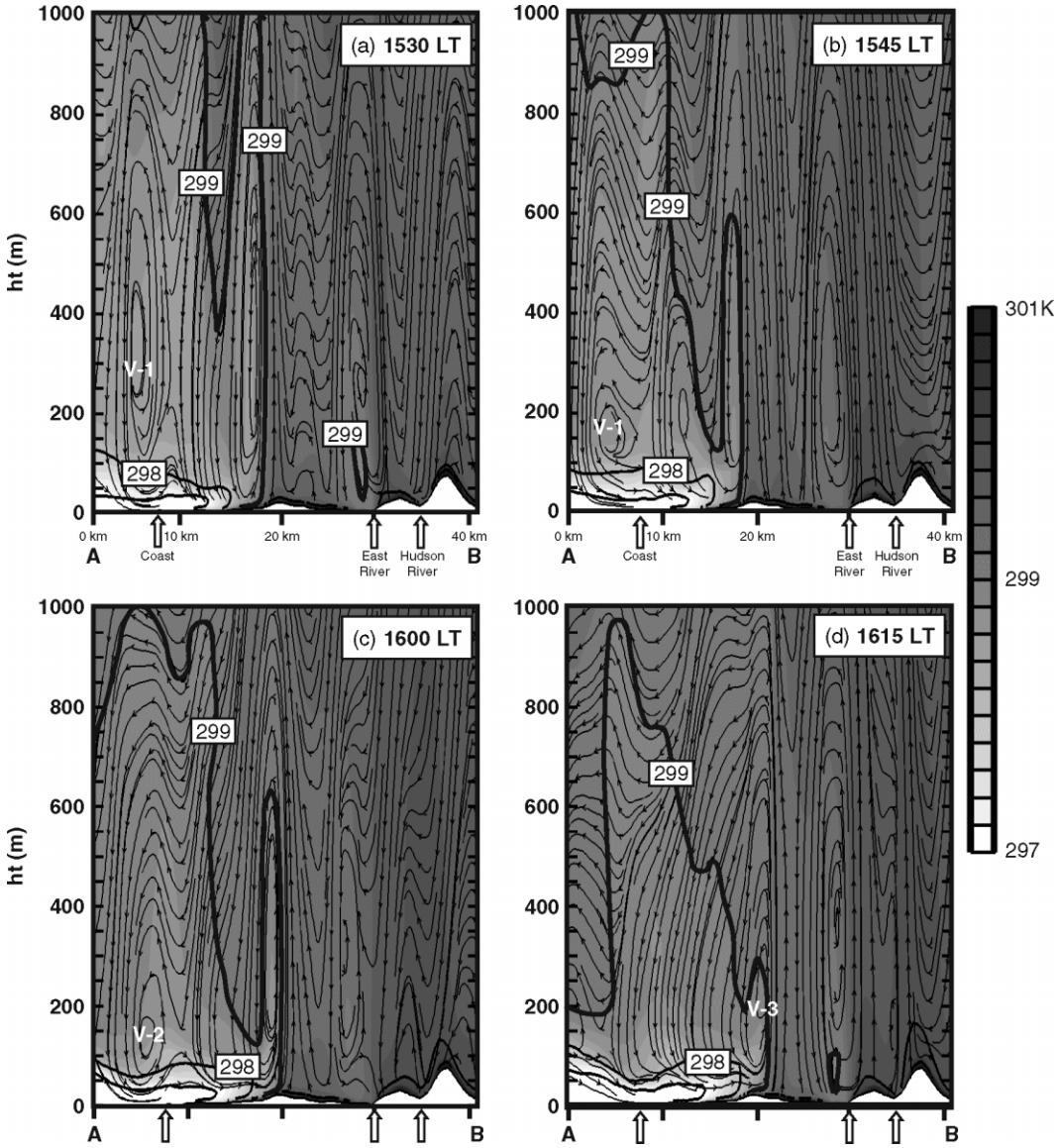

Figure 8. COAMPS nest 5 (0.444 km) cross-section along line A–B of potential temperature (shaded, interval = 1 K) and wind streamlines in the plane of the cross-section valid at (a) 1530 LT; (b) 1545 LT); (c) 1600 LT; and (d) 1615 LT 9 August 2004. The 299 K potential temperature contour is given in bold. Three vortices are labelled V-1, V-2, and V-3. The locations of the coastline, East and Hudson Rivers are indicated by the arrows along the abscissa, with Manhattan lying between the East and Hudson Rivers.

The results in the present study also show evidence of periodic vortex structure along the upper surface of the dense fluid (Figure 8(a)–(d)). These results appear to be consistent with KHI. Figures 8(a)–(d) bear a strong resemblance to those shown in previous investigations of KHI. In particular, the vortices discussed above are similar in size, distribution, and location relative to the density current head to those discussed by Sha *et al*. (1991) and Rao *et al*. (1999). Close examination of Figure 8(b) indicates that the wavelength of the disturbances is ∼4 km, which is well within the range of values reported in the literature. Cross-sections of Ri in the plane A–B at 1600 LT (Figure 9) indicate a broad region in which $0 < \mathrm{Ri} < 0.25$ near the head of the density current and extending back over the dense fluid in the region in which the vortices form, much as in the study by Sha *et al*. (1991), although the region in which $0 < \mathrm{Ri} < 0.25$ is more extensive than that in that two-dimensional study. Rao *et al*. (1999) report values of Ri in the Florida study in the range from 0.15 to 0.4. Furthermore, denoting the left-hand side of inequality (4) as δ, a cross-section of δ at 1600 LT (Figure 10) indicates that there is a small region within the inversion at the upper surface of the dense air in which $0 < \delta < 2$, demonstrating the existence of a flow regimen in which KH instability can occur. This further supports the contention that KHI is taking place in the simulation. In addition, the cold dense air moves with the gravity current head into New Jersey, indicating that the disturbance is not a solitary wave as in Wood *et al*. (1999).

It is noteworthy that the first evidence of KHI appears as the head of the density current interacts with the urbanized area, suggesting that the drag induced by the

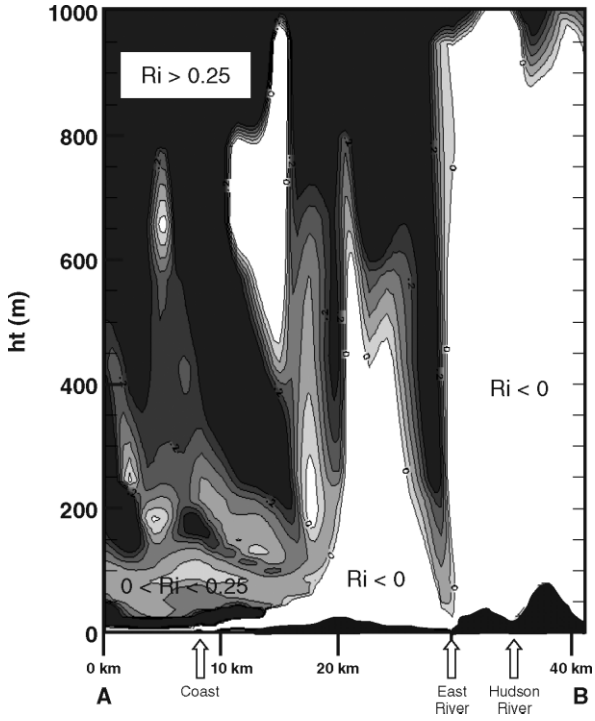

Figure 9. COAMPS nest 5 (0.444 km) cross-section along line A-B of gradient Richardson number (Ri) valid at 1600 LT 9 August 2004. Contours are given for $0 < Ri < 0.25$ (interval = 0.05) with $Ri > 0.25$ dark shading, and $Ri < 0$ no shading.

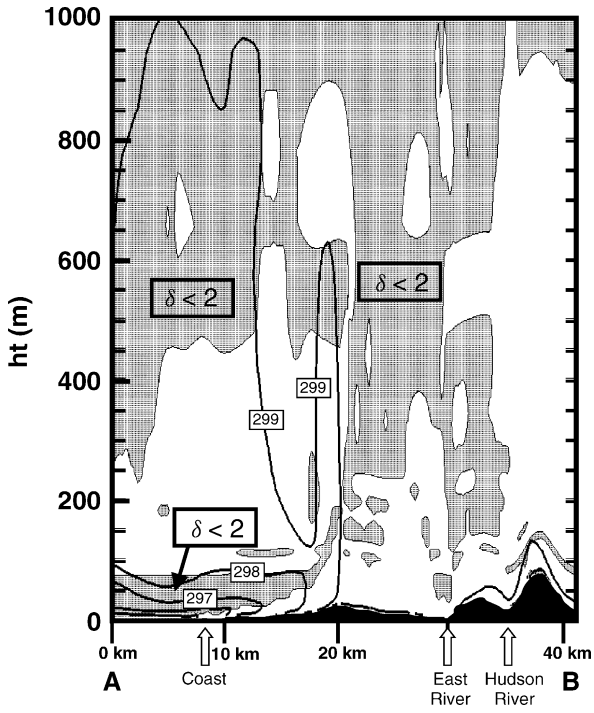

Figure 10. COAMPS nest 5 (0.444 km) cross-section along line A–B of potential temperature (contour interval = 1 K) and d (left hand side of Equation (4)) ($\delta < 2$ shaded) valid 1800 LT 9 August 2004.

urban influence may play a role in KHI by potentially modulating the depth of the head. This topic will be explored in greater detail in section 3.5 below.

3.4. Impact of the sea breeze front on plume dispersion

To assess the impact of the SBC on plume dispersion, a series of simulated continuous passive tracer releases is conducted. Releases of 200 kg s^{-1} are made at five locations, four of which are distributed over the urban area (the fifth is over the ocean near the shore (see Figure 11(a)) at the lowest model level (2 m) above ground level (AGL). Releases begin at 0800 LT (the beginning of the simulation) and show the impact of sea breeze frontal passage at four of the locations (locations 2–5). The plumes (visualized as isosurfaces of 1 mg m^{-3} concentration values) initially begin to move toward the SE, gradually shifting to a more easterly direction and then abruptly shifting to the north as the sea breeze passes each in turn. In addition to a reversal in the direction of plume motion, rather dramatic re-distribution of plume material in the vertical takes place. The large ascent at the head of the density current results in large vertical advection of tracer material. This is similar to the process described by Lyons *et al*. (1995) as 'translocation'. In that study of a Lake Michigan lake breeze, tracer material was advected to over 1 km by updraughts associated with the lake breeze front. The tracer material remained in an elevated reservoir for the remainder of the period. This appears to be the case in the present study as indicated by high dosage values in an elevated layer (not shown). The result of this translocation is a brief reduction in near-surface concentration to near zero immediately in advance of the SBC. The plume from location 2 in Brooklyn shows the impact of vertical advection (Figure 11(b)). Note the narrow 'chimney' of tracer material with the elevated reservoir above. At this time, the near-surface concentration is non-zero only over a very small area in the immediate vicinity of the release location. After passage of the SBC, however, the plumes are released into the shallow layer of dense fluid and confined to remain near the surface, greatly increasing near-surface concentration (Figure 12). The narrow, shallow plume structures persist as the plumes move across New Jersey and New York until they exit the domain to the NE.

During this period, there is substantial fine structure in the upper surface of the plume, evidently due to enhanced mixing resulting from KH billows along the upper surface of the dense air, as discussed by Sha *et al*. (1991), Rao *et al*. (1999) and Miller *et al*. (2003). To examine this process further, a series of releases are conducted at several different elevations at a location over Brooklyn (location 3). Releases are made at 2 m (as discussed above), 50 m, 106.5 m, 279 m, and 489 m AGL.

Before the passage of the sea breeze, the plumes are very similar in appearance owing to strong mixing. The plume of the passive tracer released at 489 m is quickly mixed to the surface and extends no higher than the tracer released at 2 m (not shown). After passage of the front, the plumes separate and become more distinct from one another. The plume of the tracer released at 489 m

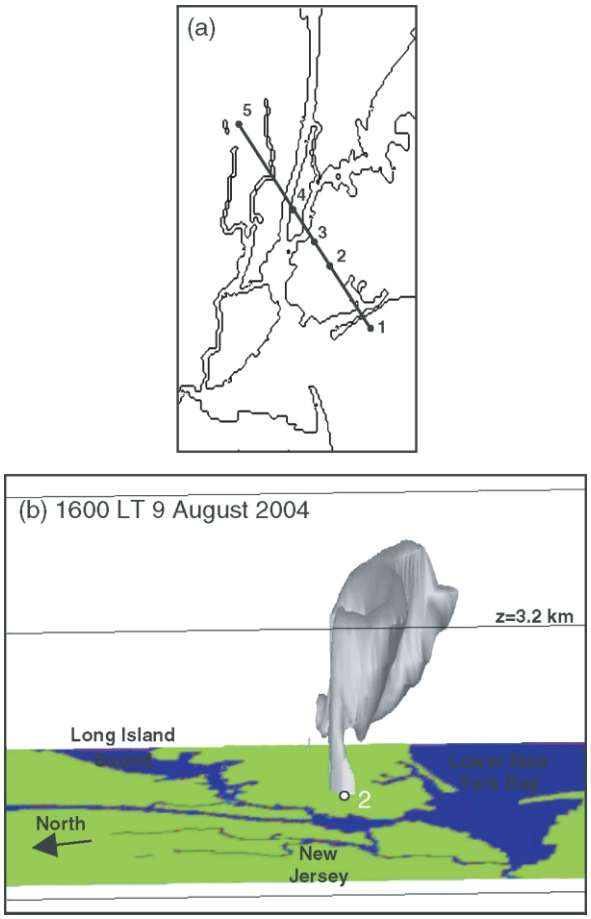

Figure 11. (a) Location of release points for five passive tracers; (b) three-dimensional visualization of COAMPS nest 5 (0.444 km) passive tracer 1 mg m^{-3} isosurface for continuous 2 m above ground level release from site 2 valid 1600 LT 9 August 2004 (view from west). The top of the box is 3.2 km.

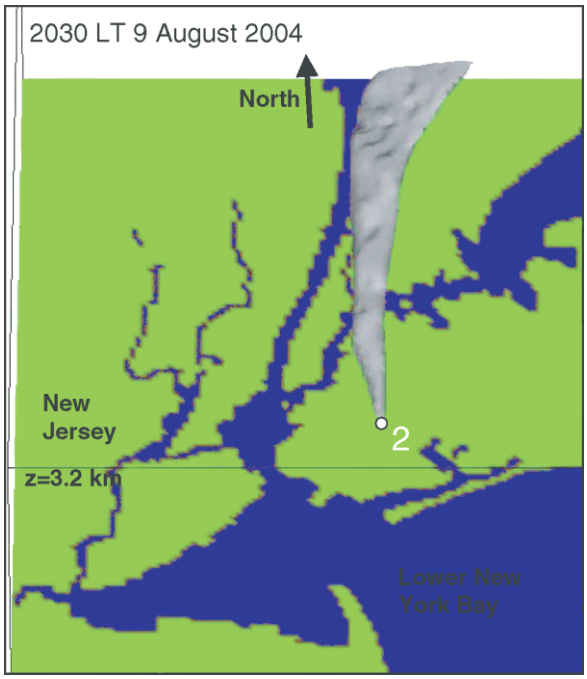

Figure 12. Three-dimensional visualization of COAMPS nest 5 (0.444 km) passive tracer 1 mg m^{-3} isosurface for continuous 2 m above ground level release from site 3 valid 2030 LT 9 August 2004 (view from south) similar to Figure 11. The top of the box is 3.2 km.

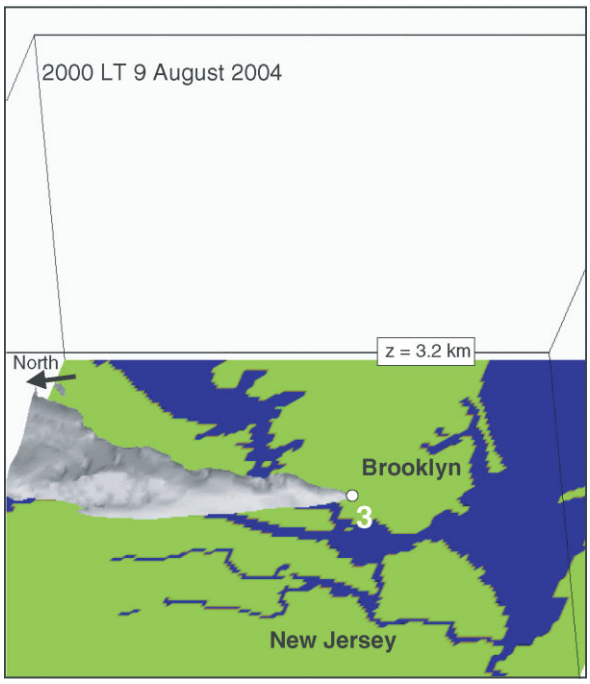

Figure 13. Three-dimensional visualization of COAMPS nest 5 (0.444 km) passive tracer 1 mg m^{-3} isosurface for continuous 106.5 m above ground level release from site 3 valid 2000 LT 9 August 2004 (view from west) similar to Figure 12.

remains well above the surface after frontal passage. The plume of the tracer released at 279 m exhibits distinct behaviour in that it is elevated near the source and then extends to the surface, giving it *the appearance of fumigation*. What is actually occurring, however, is that the tracer material in the lowest few tens of metres is simply advected to the north while the plume itself remains aloft, and is not mixed into the stable layer. Thus, the point of apparent fumigation moves continuously further from the source. The plume showing the most evidence of mixing is the one resulting from the tracer released at 106.5 m (Figure 13). The upper surface of this plume shows 'hills and valleys', which seem to appear and disappear in quasi-periodic fashion.

Trajectories launched over the urban area near location 3 show similar behaviour (not shown). Trajectories launched at low levels just before the arrival of the sea breeze front ascend rapidly and turn towards the east, exiting the domain after 2–3 h. Trajectories launched at low levels just after the passage of the sea breeze front move rapidly towards the north with little or no vertical displacement. Trajectories launched just after passage of the sea breeze front at ~100 m elevation move rapidly to the north, exhibiting large vertical displacement over a short segment of the trajectory. This is evidently the result of positive and negative vertical accelerations over short periods due to KHI.

Published in 2007 by John Wiley & Sons, Ltd.

3.5. Sensitivity to urban canopy parameterization

To assess the influence of the parameterized urban canopy on the results, a 24 h simulation is performed in which the urban land use category is set to grassland, removing all urban effects. This change in land use is applied to all urban areas and not just Manhattan. In this "no-urban" simulation, the urban area has the same surface roughness and albedo as grassland and the surface characteristics are consistent with this land use category. The initial conditions are identical to those in the control simulation described above in section 3.2. Thus, this simulation starts with the urban effects of the previous 5 days of data assimilation just as the control simulation.

The sea breeze front moves onshore at 1200 LT (Figure 14(a)) and then moves very slowly until 1500 LT, just as in the control simulation. In both simulations, the front is essentially stationary from 1300 LT to 1500 LT. Figure 14(b) shows the no-urban simulation at 1400 LT. Some intriguing differences are apparent at this time related to the local-scale SSW sea breeze. In

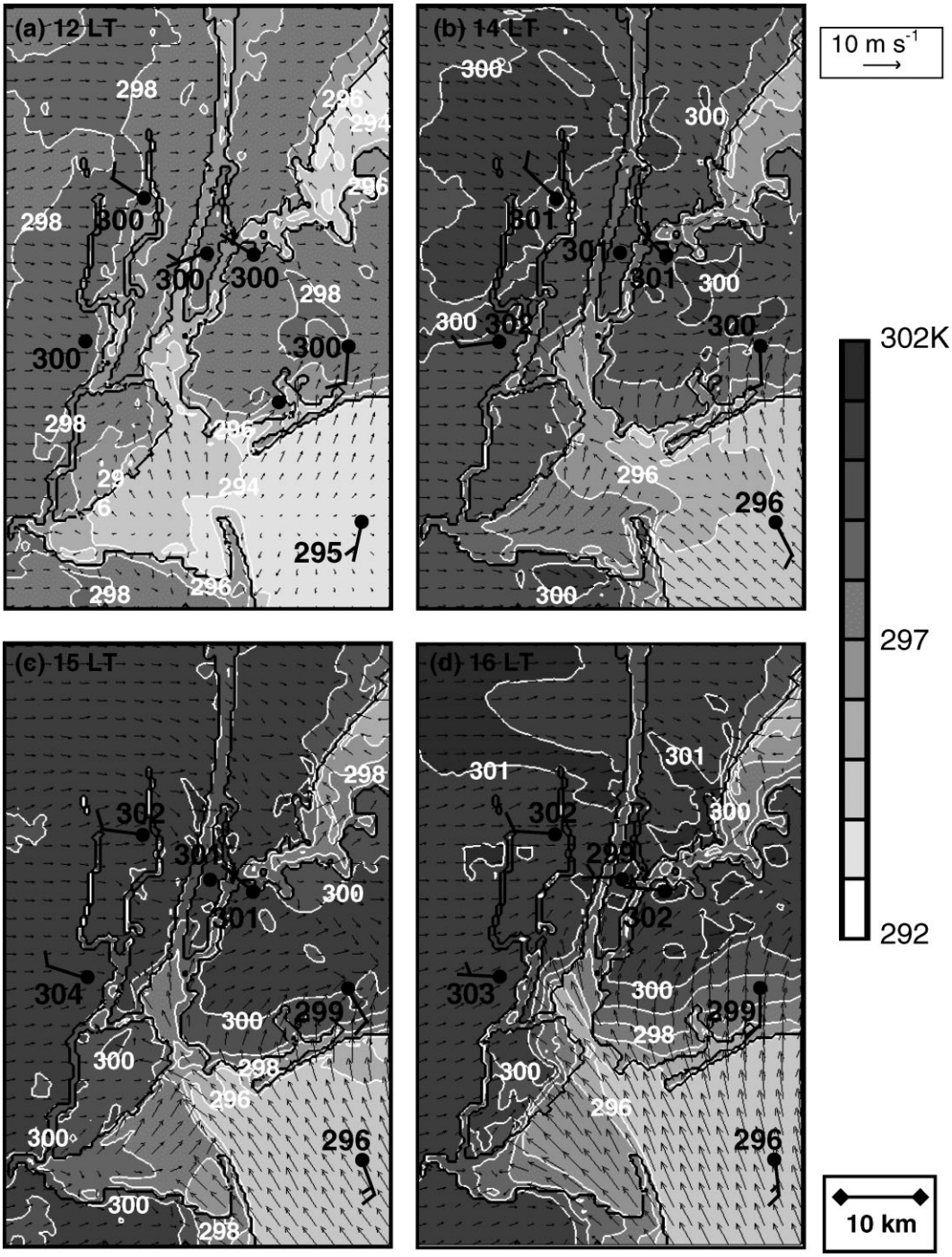

Figure 14. COAMPS nest 5 (0.444 km) no-urban simulation of 2 m potential temperatures (shaded, interval = 1 K) and 10 m winds (arrows, every fifth grid point) valid at (a) 12 LT; (b) 14 LT); (c) 15 LT; and (d) 16 LT 9 August 2004, similar to Figure 4. Observations are plotted in black (temperature, K; winds full barb = 5 m s^{-1}). (LT is UTC − 4 h).

Published in 2007 by John Wiley & Sons, Ltd.

DOI: 10.1002/qj

the no-urban simulation, the large-scale SE sea breeze reaches the coast by this time and flows though the narrows into the harbour area, effectively isolating the local-scale sea breeze. The front begins to advance inland at 1400 LT. This does not occur in the control simulation until 1500 LT. At 1500 LT (Figure 14(c)), the front moves fairly rapidly across the city at about 150% of the speed of the control simulation, reaching the midpoint of the area between the coast and Manhattan Island by 1600 LT (Figure 14(d)). The front moves smoothly past Manhattan Island with no indication of any perturbation in the flow over the meadows of Manhattan. At 1700 LT the front accelerates and reaches the northern boundary of the domain more than an hour earlier than in the control. Figure 15 summarizes the frontal motion showing isochrones for this simulation (isochrones for the control are shown for comparison).

Shown in Figure 16 is the difference in near-surface (2 m) potential temperature between the control simulation and the no-urban simulation at 1400 LT. Over most of the domain, the difference is positive, indicating that the near-surface temperature in the control is warmer than in the no-urban simulation, as might be expected. The largest positive values in the region of the SBC are near Staten Island (2.8 °C) and along the coast in Brooklyn (1.6 °C) and Queens (2.0 °C). The large values near Staten Island are due to the early arrival of the SW large-scale sea breeze, which displaces a warm tongue over the ocean near Sandy Hook and results in cool, onshore flow over the northern portion of Staten Island. Although these effects are rather subtle, they produce a large signal in the difference field. The large values along the coast in Brooklyn and Queens result from the sea breeze moving further inland in the no-urban simulation so that the air temperature is cooler than in the control.

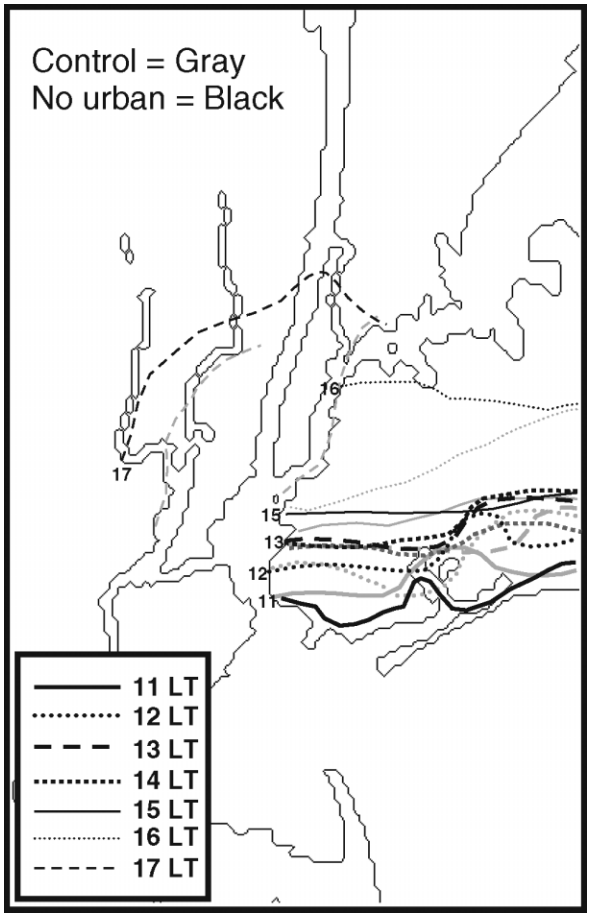

Figure 15. Isochrones of sea breeze frontal passage from 1100 to 1700 LT 9 August 2004 for COAMPS nest 5 (0.444 km) control (gray) simulation and no-urban simulation (black) similar to Figure 5.

Cross-sections in the plane A–B for this simulation are quite different from those for the control (not shown). Table II tabulates the ratio of the depth of the head to that of the following flow for this simulation and for the control. Note that the ratio ranges from 2.00 to 3.24 while in the control the ratio ranges from 2.47 to 7.35. In the control, the ratio is less than three at two times while, in the no-urban simulation, the ratio is less than three for five of the times shown. Thus, the reduced surface drag in the no-urban simulation has dramatically reduced the depth of the head relative to the following flow. Other differences between the two simulations include the reduction in the strength of the inversion above the following flow and the greater depth of the following flow. These differences between the two simulations result in an absence of KHI in the no-urban simulation.

Continuous passive tracer releases are also performed in the no-urban simulation at the same locations as used in the control. The overall pattern of plume behaviour before the passage of the sea breeze is similar to that in the control. After passage of the SBC, the upper surfaces of the plumes are relatively smooth, in contrast to the control, in which the plumes appear to be undergoing turbulent mixing at this time. In both simulations, the upper portion of the plume near the source takes on a shelf-like appearance as it spreads toward the east owing to low-level wind shear. This effect is much more pronounced in the control simulation owing the effect of the urban canopy. Thus, the overall behaviour of the tracer plumes in the control and no-urban simulations is similar before the passage of the sea breeze front. After passage of the front, the effects of low-level wind shear

Table II. Ratio of the depth of the head to that of the following flow.

Time (LT)	Control	No-urban
1500	7.35	2.59
1515	7.35	2.00
1530	5.95	2.86
1545	5.95	3.24
1600	5.95	2.59
1615	2.47	2.99
1630	2.52	3.24
1645	3.47	3.24
1700	3.58	3.00

Published in 2007 by John Wiley & Sons, Ltd.

DOI: 10.1002/qj

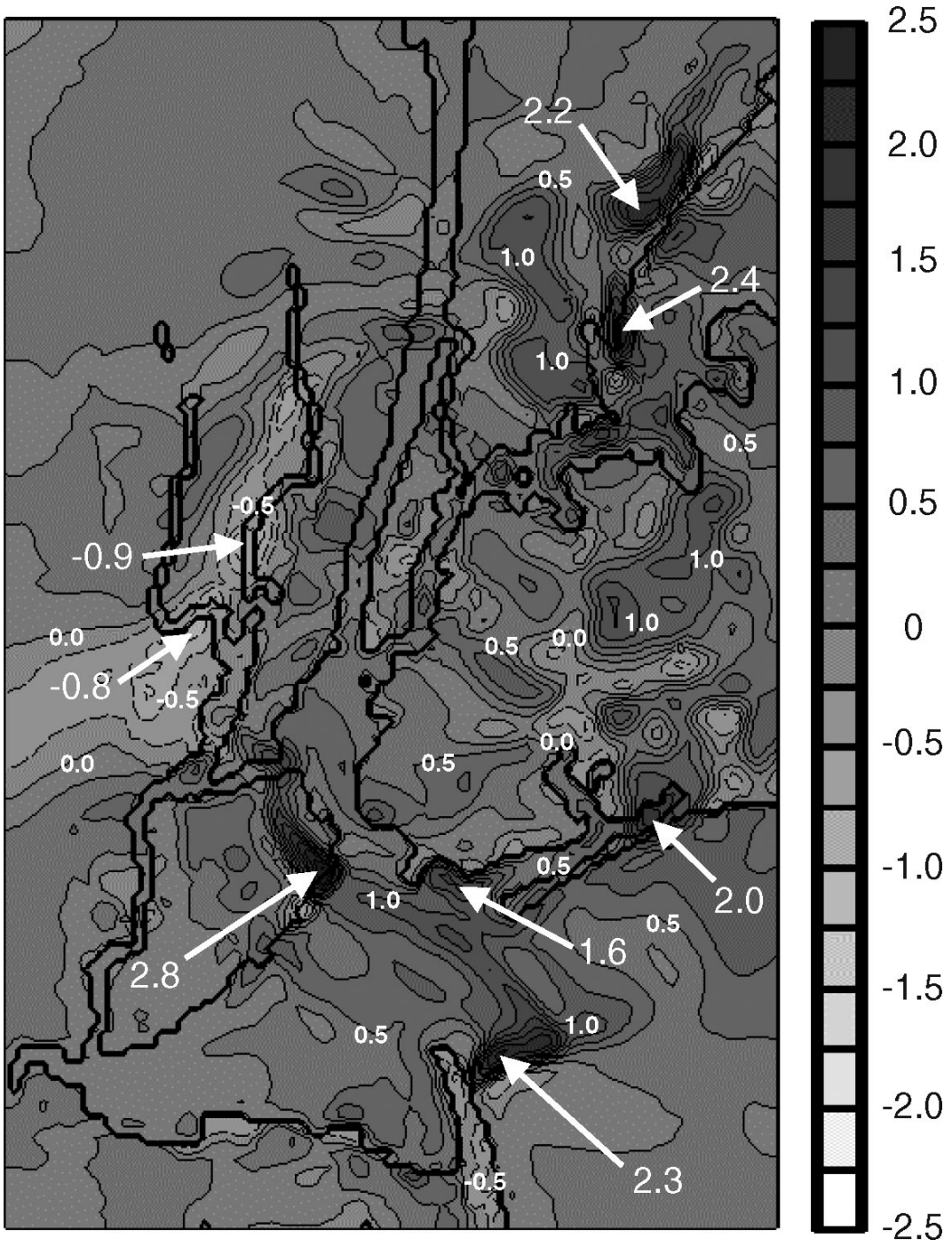

Figure 16. COAMPS nest 5 (0.444 km) 2 m potential temperature difference for control minus no-urban simulation (shaded, interval = 0.25 K) valid at 1400 LT 9 August 2004.

and turbulent mixing are more evident in the control simulation.

4. Conclusions

The two-dimensional modelling study by Sha *et al.* (1991) lays a foundation for interpreting the interaction between density currents and KHI. In the present study, the complex, three-dimensional structure of the land–sea boundaries and coastal topography introduces a number of new dynamical processes.

The three-dimensional, multiply nested, real data approach used in the present study is similar to that used by Rao *et al.* (1999) in a study of central Florida sea and river breezes. Rao *et al.* assigned different constant surface temperatures to the ocean and river surfaces and used a single 7 h simulation, with most results presented from the midpoint of the simulation (3–4 h). In contrast to that study, however, the simulations presented here were preceded by 5 days of 12 h data assimilation. Thus, the initial conditions in this study contain a rich variety of mesoscale structures while those used in the Florida study

are rather homogeneous. The present study also used the urban canopy parameterization and the high-resolution NYHOPS SST fields to provide additional mesoscale detail.

The comparison of the surface wind observations with the model forecast shows that the model captures the evolution of the SBC reasonably well. The skew-T log P thermodynamic diagrams show that the model profiles of wind speed, temperature, and moisture are in good agreement with the observations.

Our study documented the interaction of the SBC with the heavily urbanized NYC area. The comparison of the results of the no-urban and the control simulation further clarifies the nature of the interaction. The first-order effect of the urban-influenced drag and warming/cooling is to slow frontal propagation speed (Figure 13); the front reaches the East River over 1 h earlier in the no-urban simulation. This is most apparent in the isochrones shown in Figure 15. This has a number of important implications, including the effect on predictability in time and space of contaminant dispersal from sources released in the urban area (see section 3.3). The impact of the urban influence on the structure of the density current is also profound in that the depth of the head of the density current is greater than or approximately equal to about six times that of the following flow for five of the times shown in the control and approximately two to three times the depth of the following flow in the no-urban simulation (Table II). Moreover, the absence of KHI in the no-urban simulation indicates that urban drag is important in producing wind and mass distributions conducive to KHI in the model.

It should be noted that the no-urban simulation involves changing the urban land use specification only during the period of interest (a single 24 h forecast) such that the initial conditions in this simulation are the same as those in the control. An alternative approach would involve repeating the 5 days of 12 h data assimilation with the urban parameterization inactive. In this approach, the initial conditions could conceivably be quite different from the control. In particular, the boundary layer over the land could be somewhat cooler initially, possibly resulting in a weaker SBC in the no-urban simulation.

An important aspect of the present study is the impact of the SBC on contaminant plumes. Although the obvious first-order effect is a change in the direction in which the plume travels, the significant re-distribution of the tracer material in the vertical owing to the SBC circulation has a large impact on near-surface concentrations. As the sea breeze front approaches a release location, upward motion at the front results in a decrease in near-surface concentration (Figure 11). After passage of the front, the tracer is released into the shallow density current, which restricts dispersion of the plume so that near-surface concentrations quickly increase, although turbulent mixing at the upper surface of the plume due to KHI may slightly impact near-surface concentrations (Figures 12 and 13).

Several important questions about transport and diffusion in the urban sea breeze environment remain unanswered. In the present study, continuous releases were conducted over the entire period of the simulation. Thus, we did not investigate the impact of different release times on resultant concentrations. In simulations with even greater horizontal resolution, investigations of more closely spaced release points might lead to risk mitigation strategies in the event of a release of hazardous material.

The local imprint of the SBC in the NYC region displays sensitivity to the level of urbanization. The enhanced urban drag and warming/cooling are associated with increased mixing and KHI, as shown here. Other cities throughout the world are also rapidly growing, complex coastal urban centres. Though the cities may differ in particulars of morphology, it is likely that the occurrence of urban-induced features such as deeper density current heads, KHI, and translocation in contaminant dispersion will become more ubiquitous globally.

Acknowledgements

We thank Steve Burian for supplying the 250 m NYC urban database and Alan Blumberg for making available the NYHOPS SST fields. This work was partially supported by the Department of Homeland Security Urban Dispersion Program through grants P4CF40592 and P5CH40318. This study was made possible, in part, owing to the data made available by the Meteorological Assimilation Data Ingest System (MADIS) operated by the NOAA Earth System Research Laboratory Global Systems Division. We also thank three anonymous reviewers for their constructive criticism.

Appendix A

As noted in the 'Introduction', KH billows are unstable to certain wind and mass configurations. To assess the stability of the flow, the Taylor–Goldstein equation for the vertical structure of vertical velocity (w) can be used. Following Nielsen (1992), the Taylor–Goldstein equation is given by:

$$\frac{\partial^2 w}{\partial z^2} + \Lambda(z) w = 0, \tag{A1}$$

where

$$\Lambda(z) = \frac{N^2}{(U-c)^2} - \frac{\partial^2 U \Big/ \partial z^2}{(U-c)} - k^2, \tag{A2}$$

and where N is the Brunt–Vaisala frequency, U is the wind speed, c is the phase speed, and k is the wave number. This expression is a quadratic in $(U-c)^{-1}$. In general, for quadratic expressions of the form

$$Ax^2 + Bx + C = 0$$

The solution is given by

$$x = \frac{-B \pm \sqrt{B^2 - 4AC}}{2A}$$

Thus, in this case,

$$(U-c)^{-1} = \left[-\frac{\partial^2 U}{\partial z^2} \pm \left(\left(\frac{\partial^2 U}{\partial z^2} \right)^2 - 4N^2 k^2 \right)^{1/2} \right] (2N^2)^{-1}, \tag{A3}$$

Instability can only occur if the radicand is negative. Thus, it is apparent that instability occurs when

$$\frac{\partial^2 U \Big/ \partial z^2}{Nk} < 2. \tag{A4}$$

Neutral modes ($c_i = 0$) are vertically propagating if stratification and wavelength are large and curvature of the wind field is small. Unstable modes are prohibited unless the Richardson number (Ri) is <0.25.

References

Abbs DJ, Physick WL. 1992. Sea breeze observation and modeling: a review. *Aust. Meteorol. Mag.* **41**: 719.

Arritt RW. 1993. Effects of large scale flow on characteristic features of the sea breeze. *J. Appl. Meteorol.* **32**: 116–125.

Blumberg AF, Khan LA, St. John JP. 1999. Three-dimensional hydrodynamic model of New York Harbor region. *J. Hydr. Engrg.* **125**: 799–816.

Blumberg AF, Mellor GL. 1987. A description of a three-dimensional coastal ocean circulation model. In *Three-Dimensional Coastal Ocean Models, Coastal and Estuarine Sciences*, Heaps N (ed). Vol 4. American Geophysical Union: Washington, DC, 1–16.

Bornstein RD, Thompson WT. 1981. Effects of frictionally retarded sea breeze and synoptic frontal passages on sulfur dioxide concentrations in New York City. *J. Appl. Meteorol.* **20**: 843–858.

Brown MJ, Williams M. 1998. An urban canopy parameterization for mesoscale meteorological models. *Proceedings of the 2nd Symposium on the Urban Environment.* Am. Meteorol. Soc: Albuquerque, NM. 144–147.

Burian SJ, McKinnon A, Hartman J, Han W. 2005. *Gridded building statistics for New York City*. Final Report for Los Alamos National Laboratory, DHS NYC Dispersion Project, 1 March 2005, 16 pp.

Chin H-NS, Leach MJ, Sugiyama GA, Leone Jr. JM, Walker H, Nasstrom JS, Brown MJ. 2005. Evaluation of an urban canopy parameterization in a mesoscale model using VTMX and URBAN 2000 data. *Mon. Weather Rev.* **133**: 2043–2068.

Fan S, Blumberg AF, Bruno MS, Kruger D, Fullerton B. 2006. *The Skill of an Urban Ocean Forecast System*. 9th International Conference on Estuarine and Coastal Modeling, ASCE (in press).

Gedzelman SD, Austin S, Cermak R, Stefano N, Partridge S, Quesenberry S, Robinson DA. 2003. Mesoscale aspects of the urban heat island around New York City. *Theor. Appl. Climatol.* **75**: 29–42.

Harsvardhan R, Davies DA, Randall TG, Corsetti. 1987. A fast radiation parameterization for atmospheric circulation models. *J. Geophys. Res.* **92**: 1009–1016.

Hodur RM. 1997. The Naval Research Laboratory's coupled ocean/atmosphere mesoscale prediction system (COAMPS). *Mon. Weather Rev.* **125**: 1414–1430.

Hodur RM, Pullen J, Cummings J, Hong X, Doyle JD, Martin P, Rennick MA. 2002. The coupled ocean/atmosphere mesoscale prediction system (COAMPS). *Oceanography* **15**: 88–89.

Holt T, Pullen J. 2007. Urban canopy modeling of the New York City metropolitan area: a comparison and validation of single-layer and multi-layer parameterizations. *Mon. Weather Rev.* (in press).

Hsu SA. 1988. *Coastal Meteorology*. Academic Press: San Diego, CA, 260 pp.

Khairoutdinov M, Kogan Y. 2000. A new cloud physics parameterization in a large eddy simulation model of marine stratocumulus. *Mon. Weather Rev.* **128**: 229–243.

Kraus H, Hacker JM, Hartmann JM. 1990. An observational, aircraft-based study of sea breeze frontogenesis. *Boundary-Layer Meteorol.* **53**: 223–265.

Lapworth A. 2000. Observation of atmospheric density currents using a tethered balloon-borne turbulence probe system. *Q. J. R. Meteorol. Soc.* **126**: 2811–2850.

Loose TRD, Bornstein. 1977. Observations of mesoscale effects on frontal movement through an urban area. *Mon. Weather Rev.* **105**: 563–571.

Louis JF. 1979. A parametric model of vertical eddy flues in the atmosphere. *Boundary-Layer Meteorol.* **17**: 187–202.

Lyons WA, Sawdey ER, Schuh JA, Carby RH, Keen CS. 1981. *An updated and expanded coastal fumigation model*. Proceedings, 74th Meeting of the Air Pollution Control Association, Philadelphia, PA, 21–26 June.

Lyons WA, Pielke RA, Tremback CJ, Walko RL, Moon DA, Keen CS. 1995. Modeling impacts of mesoscale vertical motions upon coastal zone air pollution dispersion. *Atmos. Environ.* **29**: 283–301.

Miller JE. 1948. On the concept of frontogenesis. *J. Meteorol.* **5**: 169–171.

Miller STL, Kleim BD, Talbot RW, Mao H. 2003. Sea breeze: structure, forecasting, and impacts. *Rev. Geophys.* **41**: 1–31.

Nielsen JW. 1992. In situ observations of Kelvin–Helmholtz waves along a frontal inversion. *J. Atmos. Sci.* **49**: 369–386.

Novak DRBA, Colle. 2006. Observations of multiple sea breeze boundaries during an unseasonably warm day in metropolitan New York City. *Bull. Am. Meteorol. Soc.* **87**: 169–174.

Physick WL. 1980. Numerical experiments on the inland penetration of the sea breeze. *Q. J. R. Meteorol. Soc.* **106**: 735–746.

Pullen J, Holt T, Blumberg AF, Bornstein RD. 2007. Atmospheric response to local upwelling in the vicinity of New York/New Jersey Harbor. *Mon. Weather Rev.* (in press).

Rao PA, Fuelberg HE, Droegemeir KK. 1999. High resolution modeling of the Cape Canaveral area land–water circulations and associated features. *Mon. Weather Rev.* **127**: 1808–1821.

Reible DD, Simpson JE, Linden PF. 1993. The sea breeze and gravity current frontogenesis. *Q. J. R. Meteorol. Soc.* **119**: 1–16.

Rutledge SA, Hobbs PV. 1983. The mesoscale and microscale structure and organization of clouds and precipitation in midlatitude cyclones. VIII: A model for the seeder-feeder process in warm frontal rainbands. *J. Atmos. Sci.* **40**: 1185–1206.

Sha W, Kawamura T, Ueda H. 1991. A numerical study on sea/land breezes as a gravity current: Kelvin–Helmholtz billows and inland penetration of the sea-breeze front. *J. Atmos. Sci.* **48**: 1649–1665.

Simpson JE, Mansfield JDA, Milford JR. 1977. Inland penetration of sea breeze fronts. *Q. J. R. Meteorol. Soc.* **103**: 47–76.

Stull RB. 1988. *An Introduction to Boundary Layer Meteorology*. Kluwer Academic Publishers: Boston, MA, 666 pp.

Wood R, Stromberg JM, Jonas PR. 1999. Aircraft observations of sea-breeze frontal structure. *Q. J. R. Meteorol. Soc.* **125**: 1959–1995.

Yamada T. 1978. *A three-dimensional second-order closure numerical model of mesoscale circulations in the lower atmosphere: description of the basic model and application to the simulation of the environmental effects of a large cooling pond*. Argonne National Laboratory Report ANL/RER-78-1 : Argonne, IL, 67 pp.

Zhong SES, Takle. 1992. An observational study of sea- and land-breeze circulation in an area of complex coastal heating. *J. Appl. Meteorol.* **31**: 1426–1438.